



October 2005

Comparison of Computational and Experimental Aerodynamics: Results for a WMU Solar Car Model

Yang Yang
Western Michigan University

William W. Liou
Western Michigan University

Follow this and additional works at: <http://scholarworks.wmich.edu/hilltopreview>

 Part of the [Mechanical Engineering Commons](#)

Recommended Citation

Yang, Yang and Liou, William W. (2005) "Comparison of Computational and Experimental Aerodynamics: Results for a WMU Solar Car Model," *The Hilltop Review*: Vol. 1: Iss. 1, Article 6.

Available at: <http://scholarworks.wmich.edu/hilltopreview/vol1/iss1/6>

This Article is brought to you for free and open access by ScholarWorks at WMU. It has been accepted for inclusion in The Hilltop Review by an authorized administrator of ScholarWorks at WMU. For more information, please contact maira.bundza@wmich.edu.



Comparison of Computational and Experimental Aerodynamics Results for a WMU Solar Car Model

YANG YANG

AND

WILLIAM LIOU, PH.D.

Department of Mechanical and Aeronautical Engineering
Western Michigan University

ABSTRACT

Three-dimensional numerical simulations using FLUENT [1] were performed to model the airflow over the Sunseeker, an award-winning solar car that was designed and built at Western Michigan University. Converged numerical solutions on three different grids are reported and compared with the available experimental data, which include the lift and the drag coefficients. Also reported are the results obtained by using the second-order upwinding discretization on one of the grids. The comparison shows that the computed lift coefficients agree well with the experimental data for all the three grids and the different orders of numerical methods, indicating that the pressure field is well captured. The agreement with the data for drag coefficient varies, which appears to suggest a higher degree of dependency on the grid distributions than that for the lift coefficient. These results are discussed in terms of their implications for the simulations of similar low-drag vehicles.

INTRODUCTION

Western Michigan University's (WMU) Sunseeker solar racecars have participated in a series of American Solar Challenge, a biannual competition with about 20 teams participating in each race since 1990. These represented colleges and universities from across the United States and Canada. In the latest race in July 2003, the Western team earned fifth place in the 2,300-mile race.

The WMU Sunseeker has three main parts: the canopy, the upper surface that is covered with an array of solar battery cells, and the chassis. Figure (1) shows a photo of the 2003 team and the Sunseeker car that was simulated here. The Sunseeker is 196.25 inches in length and 68.75 inches in width. The top speed can reach 70 mph running solely on the solar energy provided by the solar panels on the upper surface.

One of the emphases considered when the solar car was designed was achieving low aerodynamic drag. The design also must provide enough upper surface area for the solar panels and enough volume space to house the driver and the motor. Wind-tunnel testing of the Sunseeker model has been performed at two industrial facilities and also in the Applied Aerodynamics Laboratory at WMU. In the WMU subsonic wind tunnel, a 1/5 scale model was used. Figure (2) shows the setup in the test section of the tunnel. The model was bolted down to the floor of the test section with no wheels. A six-component force balance was used, and the data for the forces and the moments were obtained [2]. A smoke gun has been used in some cases to provide a visualization of the flow. There is, however, no detailed measurement on the flow properties, such as the surface pressure and the velocity distributions. There are also no data that indicate whether the boundary layers are laminar, transitional, or turbulent at the air speeds tested.

This paper reports the results of the numerical solutions of the three-dimensional flow field around the Sunseeker. Computational fluid dynamics (CFD) simulations of the flow fields around road vehicles are critical to modern-day automobile designs and many articles have been written in this area. A comprehensive review can be found in Hochu and Sovran [3]. CFD has also been used in the development of the aerodynamics characteristics of solar car is[4]. Compared with the traditional automobiles that run on internal combustion engine, the energy available for solar cars is far less. Therefore drag reduction must be a main consideration in the aerodynamic design of solar car.

From the vehicle stability point of view, it is also important to evaluate the amount and the direction of the lift. With the resources available, the WMU Sunseeker has been designed with limited use of CFD tools. Although the car has performed satisfactorily in the past races, it is important that matured CFD technologies be assessed and considered for the future designs.

The widely available commercial software FLUENT is used in this study. The computed aerodynamic characteristics of the Sunseeker, including the lift coefficient, the drag coefficients, and the surface pressure distribution will be reported and compared with the wind tunnel data. In addition, the simulated flow will be studied by examining the flow pressure and velocity distributions around the car.

SIMULATION CONDITIONS

The computational model of the Sunseeker was built based upon an IGES file that was generated by a CAD software. The topology and connectivity information about the car surfaces did not affect the manufacturing of the car parts and were not recorded in the CAD file. Therefore, the geometric information retained in the IGES files is not sufficient for CFD. To improve the quality of the geometry, we have used Pro/E to reconstruct the model. The disconnected edges and faces were “stitched” together and some poorly defined surfaces were replaced by mathematically smooth curves. As it is well known, the initial meshing of a new geometry is the most time-consuming part of a CFD simulation, when the model has to be “cleaned up”.

After the geometry was reconstructed and became numerically acceptable, the file was then imported into Gambit, an accompanying meshing software of FLUENT, to construct a three-dimensional grid system. Since this is a symmetric three-dimensional external flow problem, only a half of the Sunseeker needs to be simulated. A rectangular computational domain, as shown in Figure (3), has been used. The domain accommodates the half-car model with a symmetry plane. The car surfaces were first covered with uniformly distributed triangular mesh elements. The surfaces, combined with those from the outer block, were stitched together to form a single meshable volume of the computational domain. Tetrahedral unstructured mesh cells were used in the computational domain.

Three different grids, denoted as Grid A, Grid B, and Grid C, were used in this study. Grids A and C both employ the size function from Gambit, while Grid B uses the stretching scheme. For Grid A, the cell size gradually grow from around 0.0069 m near the car surface up to about 0.271 m in the far-field where the incoming flow is assumed undisturbed by the presence of the car. The grid distribution on the symmetry plane for Grid A is shown in Figure (4). The grid density is high around the car where the flow gradients can be large. For the same reason, there are also densely packed meshes in the clearance region between the underside of the car and the ground. Figure (5a) provides a combined isometric view of the computational mesh on both the upper surface of the car and the symmetry plane. Figure (5b) shows a cross-sectional cut (in the z-direction) of the three-dimensional volume grid. There are 131,079 nodes and 727,890 tetrahedral cells in grid A. Grid B was generated by the simple stretching method in Gambit, which resulted in a coarser mesh around the car than Grid A. Grid B has 146,112 nodes and 673,483 tetrahedral cells. It is found that the size function used in generating Grid A can effectively wrap around the car body with much densely distributed grid points than the stretching scheme used for Grid B. A third Grid C was also generated by using the same size function as that used for Grid A. The distance of size function in Grid C is about one half of that used in generating Grid A. Hence Grid C has a much coarser grid distribution near the wind tunnel floor than that of Grid A. There are 134,095 nodes and 738,882 tetrahedral cells for Grid C. The major part of the results presented in this paper has been obtained by using grid A.

The resulting mesh file was then imported into FLUENT. In FLUENT, the three-dimensional, segregated, implicit steady solver was used. The velocity inlet and pressure outlet boundary conditions were used at the inlet and the exit surfaces that are shown in Figure (3), respectively. The no-slip wall conditions were applied on all car surfaces and on the floor of the wind tunnel denoted by box wall 3. Symmetric conditions were prescribed for both the symmetry plane and the surfaces of box wall 1 and box wall 2. No turbulence model was invoked in the calculations. In addition to the residuals of the numerically solved governing equations, we have also monitored the lift coefficient and the drag coefficient to determine the convergence of the computations. The simulation results

were presented in terms of velocity magnitude and gauge pressure. FLUENT uses the decomposition of the absolute pressure into the operating part and the gauge part to reduce the round-off errors when calculating low-speed flows; hence the pressure values presented in this report are all gauge values. The operating pressure has been set equal to the atmospheric pressure.

In the simulations, the test model was attached to the floor at the bottom of the wheel cover with a ground clearance of 1.6 inch. The air at room temperature has an incoming airspeed of 2.0 miles/hour. The Reynolds number based on the longitudinal length of the car is in the order of. This corresponds to the lowest Reynolds number used in the wind tunnel testing. The simulations have been performed on a laptop computer with a 2.2 GHz Pentium 4 CPU and 640 MB memory. The run time is normally around 7 hours for roughly 600 iterations.

SIMULATION RESULTS

The first-order upwinding method has been used in all the three grids and the numerical solutions were found to have converged for all of them. The less numerically dissipative second-order upwinding method in FLUENT was also activated for a simulation using Grid A. The evolutions of the residuals for the run with the second-order upwinding method are shown in Figure (6). The numerical simulation took about 600 iterations for the residual of the continuity equation to drop by about five orders of magnitude and was therefore considered converged.

The numerical lift coefficient evolutions during the iterations are shown in Figure (7) for all the cases calculated. The values of the calculated lift coefficients level out after about 400 iterations in all the calculations performed, although the calculations continue until all the residuals of the equations have dropped by five orders of magnitude. The measured lift coefficient C_L is also included in Figure (7) for comparison. The lift coefficients have been normalized by the free stream dynamic pressure and the frontal area. The negative value of means that a downward force toward the ground is exerted on the car at this speed, which improves the cornering capability of the car [5]. The converged calculated lift coefficients using Grids A, B, and C compare well with the measured value. The differences between the numerical results and the measured data range from 4.7% for Grid A to 10% for Grid B. The result obtained by using the second-order upwinding method differs little from that using the first-order upwinding. The reasonably good agreement between the various calculated lift coefficients and the measured value indicates that the pressure field, which is the main contributor to lift for the current flow condition, has been adequately resolved. In other words, the outer “inviscid” part of the flow field around the car, which determines the car surface pressure, has been accurately simulated.

Figure (8) shows a similar comparison of the drag coefficient. The cases and the notations are the same as those for Figure (7). The drag coefficient evolutions show that the calculated drag forces reach stationary values at nearly the same pace as those for the lift. The converged values, however, vary. The Grid A and the Grid C results agree very well with the measured value of 0.24. The result of the second-order scheme is somewhat lower than that of the first-order scheme. For Grid B, which has the coarsest surface meshes among the three grids used, the calculated drag coefficient deviates significantly from the measured value. The variation in the drag calculations points to a need to examine the calculated boundary layer on the car surfaces. A careful examination of the grids and the flow field solutions shows that, over some parts of the vehicle surfaces, the boundary layers are poorly resolved with only a few grid points inside the viscous dominated regions.

The pressure distributions on the surfaces of the car has been examined and presented in Figure (9). The regions of high pressure appear at the leading edge and the front wheel casings of the car. The similar high-pressure area can also be spotted near the canopy, which extrudes from the upper surface of the car. The airflow experiences resistance at these locations, hence it is expected that the pressure increases when velocity drops. From Figure (9), we can see that the flow field around the whole car surfaces develops in a relatively smooth manner except for the leading edge, the front wheel casing and the bulged structure under the car, which was designed to install the driver's seat.

Figure (10) shows the velocity magnitude contours, normalized by the free stream value, on the cross-sectional plane shown in Figure (5b). The contour lines near the bottom wall of the wind tunnel show a boundary layer behavior in the near wall flow region. There is also a high-speed region above the canopy.

Another view of the velocity magnitude distribution is shown for the symmetric plane in Figure (11). The air flows from the left to the right parallel to the lower wall of the wind tunnel. The air moves along the surface of the car smoothly except nearing the region where the canopy connects to the car body, where low-speed regions are observed. The tail part of the car ends with a cusp and the flow from the upper and the lower surfaces merge smoothly. The velocity vectors and the streamline patterns have not shown flow separation in the region immediately downstream of the car body. The gage pressure (the difference between the absolute and the atmospheric pressure) contours on the symmetry plane are shown in Figure (12). Comparing with Figure (11), the highest pressure appears at the leading edge of the car where the velocity magnitude has its minimum. The lowest pressure area is on the top of the canopy where the air picks up the highest speed. The calculated quantities are consistent with the expected flow physics.

CONCLUDING REMARKS

For the initial simulations presented, we have successfully built the surface meshing of the Sunseeker test model. Converged numerical solutions for the flow field around the Sunseeker have been obtained. The calculated flow fields have been shown for three different grids and two numerical methods of different order of accuracy.

The computed lift coefficients agree well with the measured data for all the three grids. This agreement suggests that the outer, inviscid part of the flow around the Sunseeker has been adequately resolved by each and every one of the grids used and the results are accurate. The predicted drag coefficient values are less uniform, although the agreement is reasonably well for two of the cases calculated. To improve the drag force predictions, more computational cells are likely to be needed within the boundary layers that are expected to develop on the surface of the car. This measure can easily push the total number of cells over one million. Since the thickness of the boundary layer decreases with the increase of the Reynolds number, such refinements of the grid distributions in the boundary layer will become important for the higher car speeds. It is more so when transition or turbulence models are used at these high Reynolds numbers.

It should also be noted that the clearance between the underbody of the car and the wind-tunnel floor was not recorded during the testing that was carried out at the Applied Aerodynamics Laboratory of WMU. In the numerical calculations, the wheel cases were assumed to be 1.6 in above the tunnel wall. Since the two sides of the car extend toward the ground to accommodate the wheels in its original design, the spacing between the lower side of the main body and the side walls actually form an air passage that handles a significantly more amount of airflow than what one normally would see without the drop-down "side curtain". To examine the effect of the clearance, we have run a case with the car sitting higher above the wind tunnel floor. The resulting calculated lift and drag coefficient were an order of magnitude smaller than the measured values. It can be argued that the ground clearance has some level of influence on the aerodynamic characteristics of the Sunseeker and needs to be modeled in an appropriate way.

Acknowledgments

The authors would like to thank J. Jacob for his valuable support in the Pro/E applications and A. Poot for his kind assistance in access to the Sunseeker project laboratory.

References

FLUNET 5 User's Guide, FLUENT Incorporated, July 1998.

E. Pederson, "Aerodynamic Design and Testing of the 1999 WMU Solar Car," Private Communication (2003).

Hochu, W. and Sovran, G., "Aerodynamics of road vehicles," *Annual Review of Fluid Mechanics*, 25 (1993) 485.

H. Ozawa, S. Nishikawa and D. Higashida, "Development of aerodynamics for a solar race car", JSAE Review 19 (1998) 343-349.

M. Tomiyama, K. Maeda and F. Nakamura, "The development of a method to obtain the optimum lift coefficient using the vehicle dynamics analysis", JSAE Review 23 (2002) 69-74.



Figure 1. The 2003 Sunseeker and the team members. (Courtesy of Cathy Smith)



Figure 2. The experimental model of the Sunseeker sits in the test section of the WMU wind tunnel.

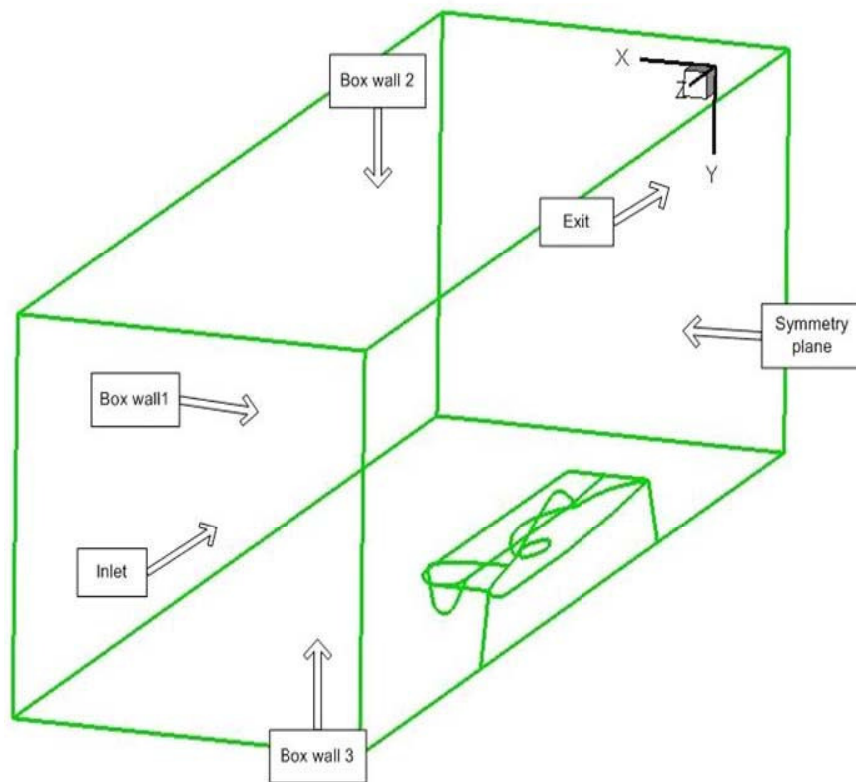


Figure 3. Configuration of the computational domain.

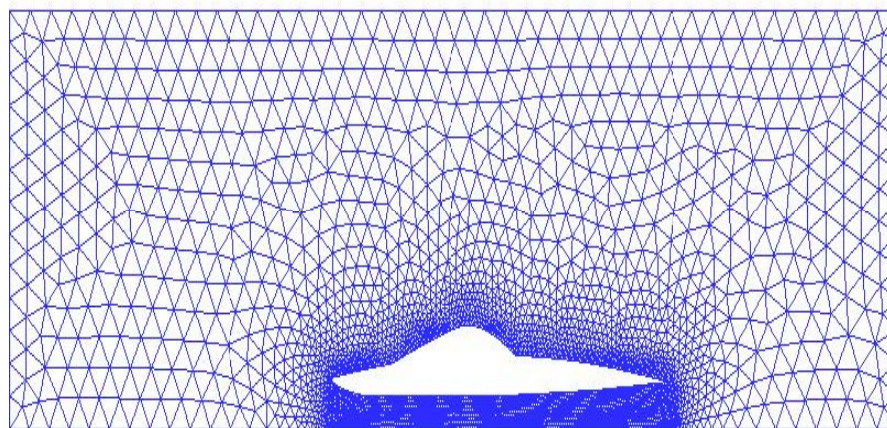


Figure 4. The tetrahedral mesh on the symmetry plane.

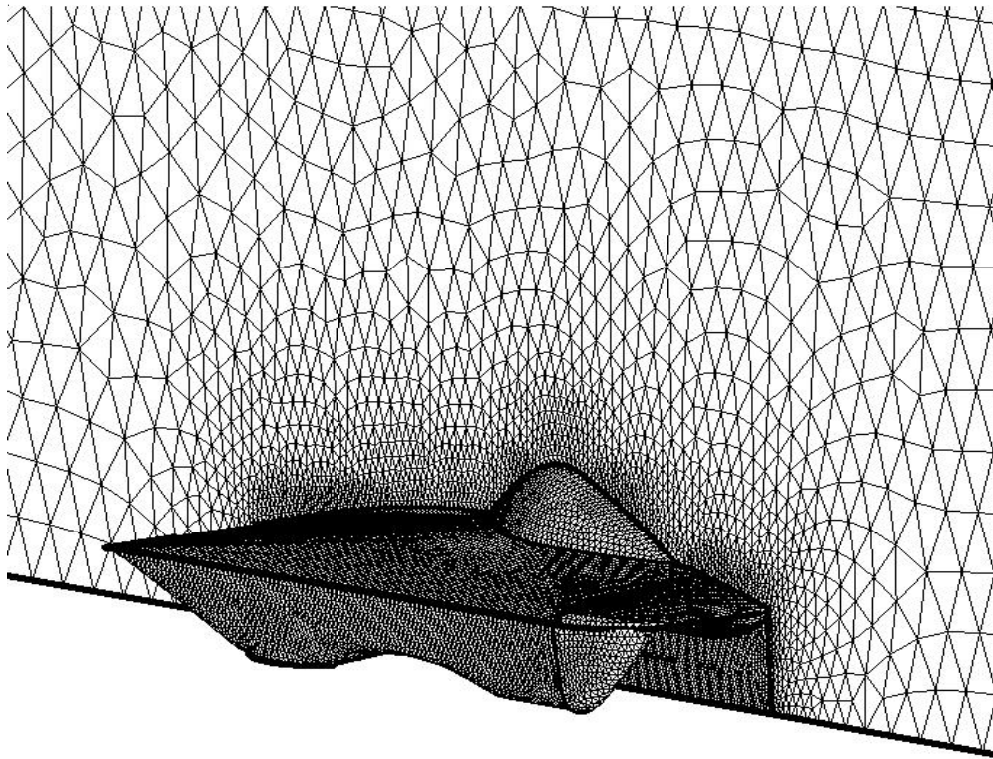


Figure 5a.

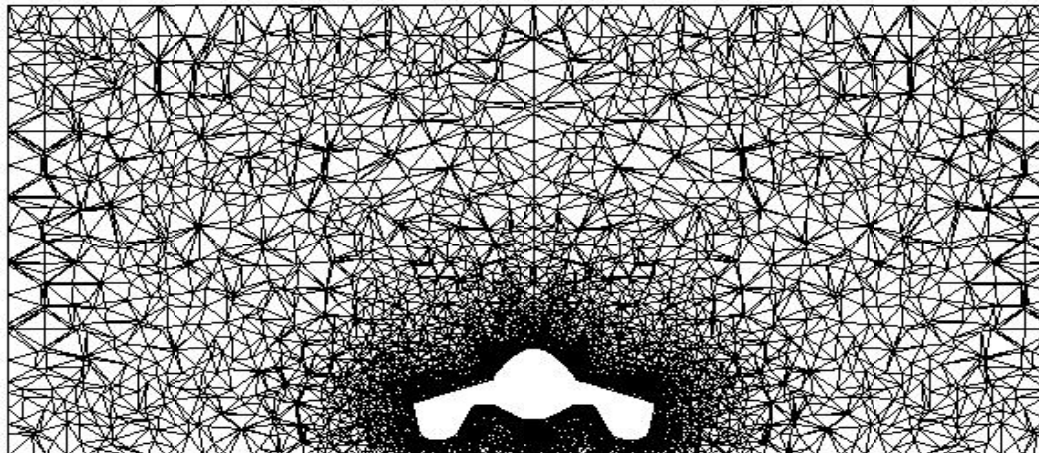


Figure 5b.

Figure 5. The tetrahedral computational mesh. (a) On the car surface and the symmetry plane. (b) On a cross-sectional plane.

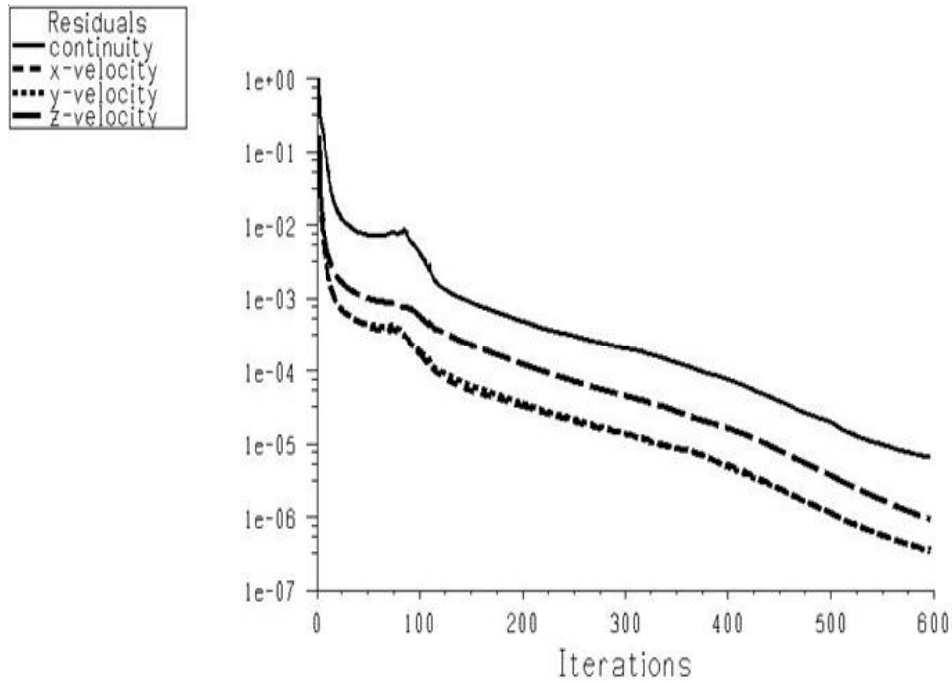


Figure 6. The variation of the residuals of the numerical solved continuity equation and the momentum equations.

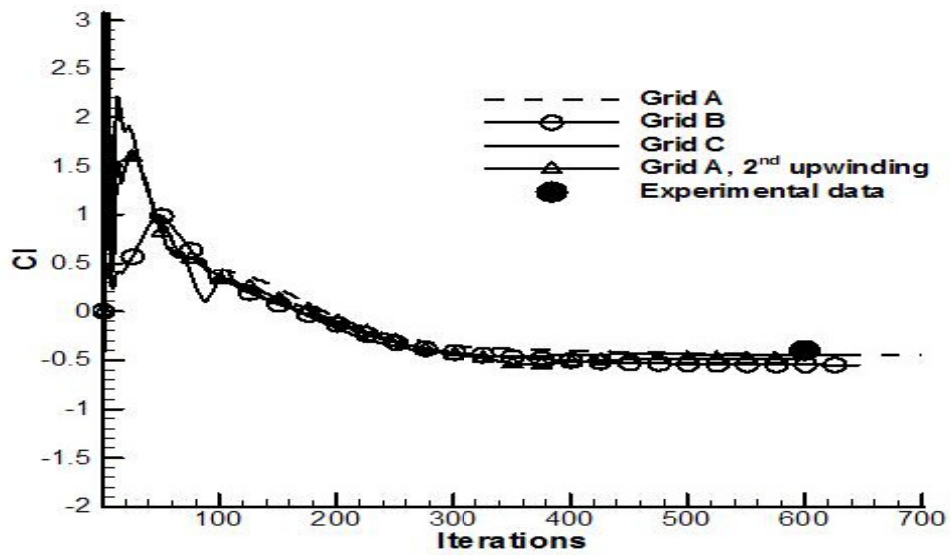


Figure 7. Convergence history of.

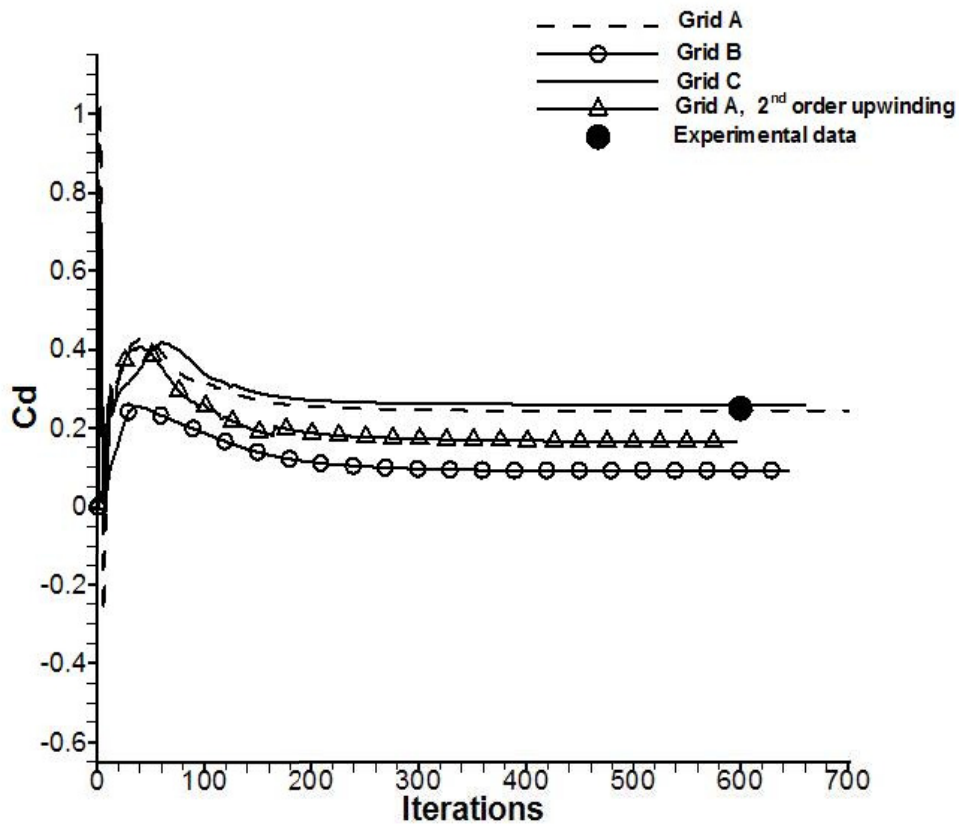


Figure 8. Convergence history of .

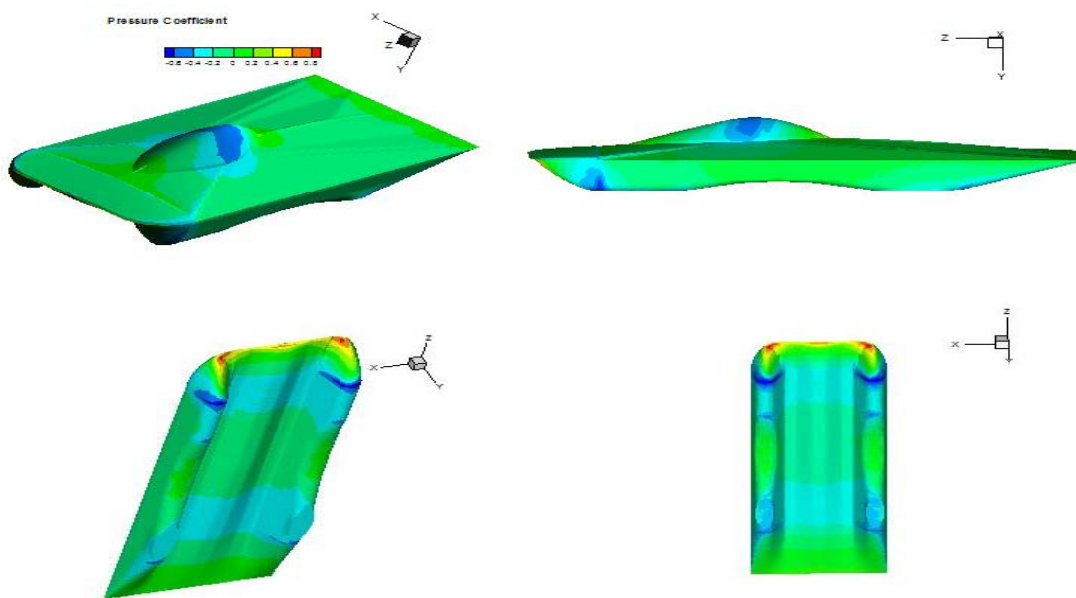


Figure 9. Different views of the surface pressure distribution on the car surfaces.

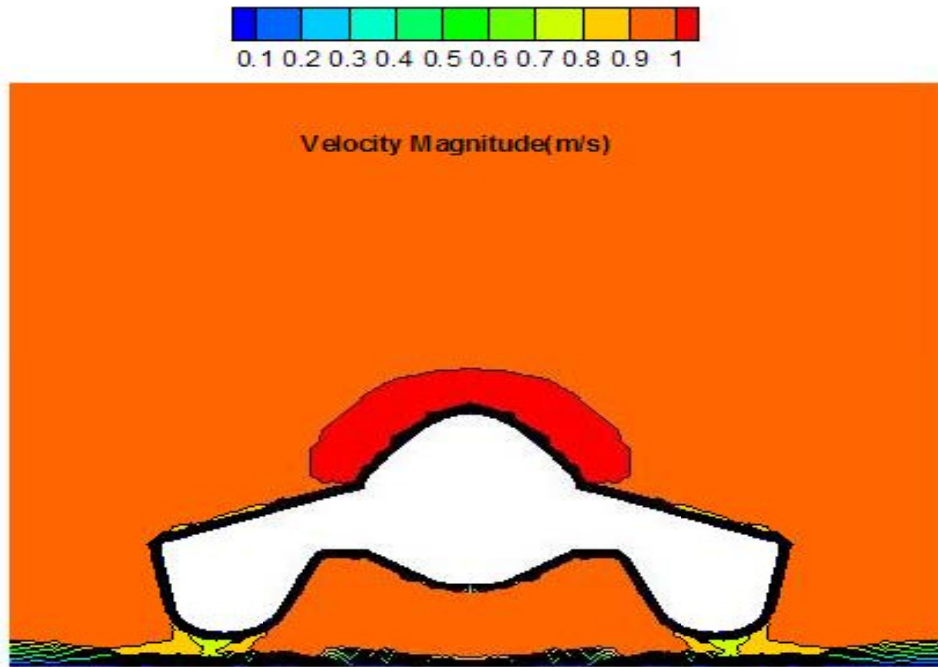


Figure 10. Velocity magnitude contours on a cross-section plane.

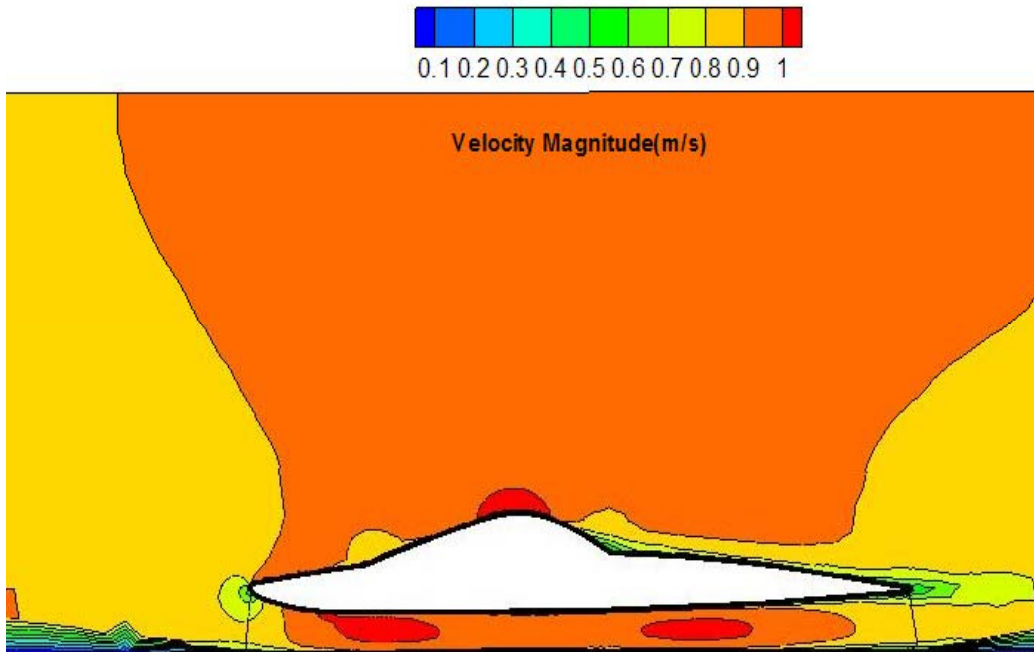


Figure 11. Velocity magnitude contours on the symmetry plane.

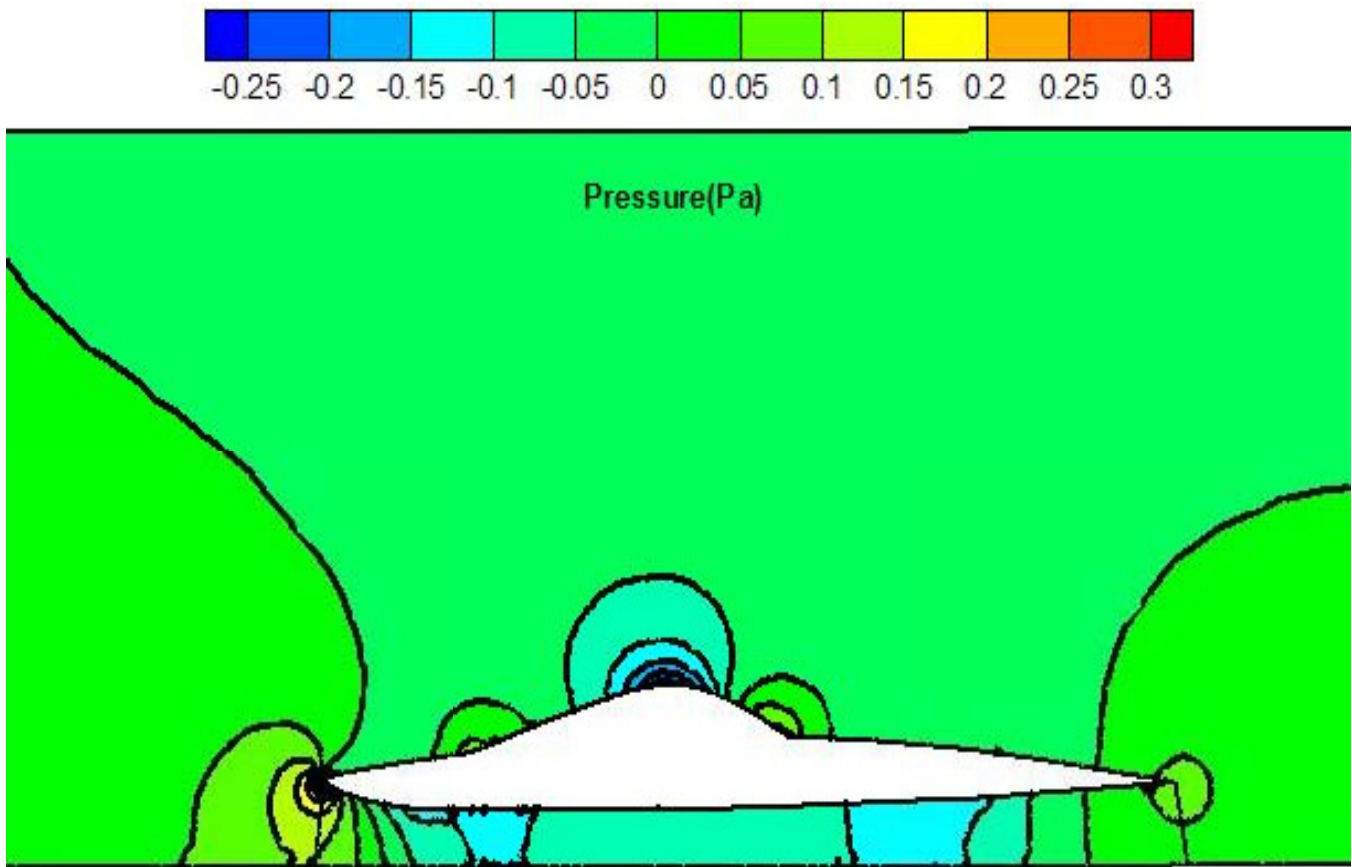


Figure 12. Pressure contours on the symmetry plane.